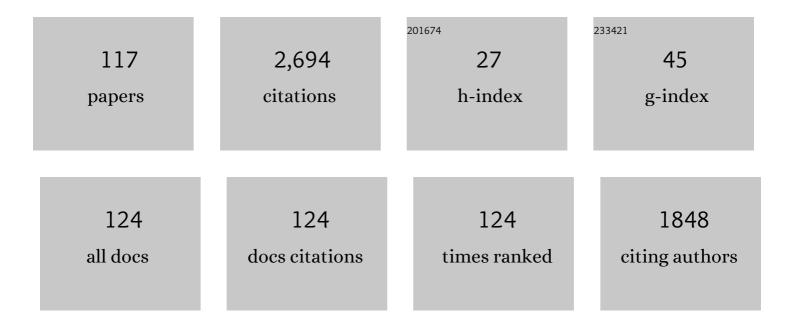
Cathryn Mitchell

List of Publications by Year in descending order

Source: https://exaly.com/author-pdf/8121664/publications.pdf Version: 2024-02-01



#	Article	IF	CITATIONS
1	History, current state, and future directions of ionospheric imaging. Reviews of Geophysics, 2008, 46, .	23.0	210
2	GPS TEC and scintillation measurements from the polar ionosphere during the October 2003 storm. Geophysical Research Letters, 2005, 32, n/a-n/a.	4.0	147
3	FOUR-DIMENSIONAL ELECTRICAL CAPACITANCE TOMOGRAPHY IMAGING USING EXPERIMENTAL DATA. Progress in Electromagnetics Research, 2009, 90, 171-186.	4.4	137
4	Bipolar climatology of GPS ionospheric scintillation at solar minimum. Radio Science, 2011, 46, .	1.6	114
5	System Design for Geosynchronous Synthetic Aperture Radar Missions. IEEE Transactions on Geoscience and Remote Sensing, 2014, 52, 7750-7763.	6.3	105
6	lonospheric electron concentration imaging using GPS over the USA during the storm of July 2000. Geophysical Research Letters, 2004, 31, n/a-n/a.	4.0	67
7	Dynamics of high-latitude patches and associated small-scale irregularities during the October and November 2003 storms. Journal of Atmospheric and Solar-Terrestrial Physics, 2008, 70, 879-888.	1.6	58
8	GPS scintillation in the high arctic associated with an auroral arc. Space Weather, 2008, 6, .	3.7	56
9	Imaging of electron density troughs by tomographic techniques. Radio Science, 1997, 32, 1607-1621.	1.6	55
10	Two-dimensional mapping of the plasma density in the upper atmosphere with computerized ionospheric tomography (CIT). Physics of Plasmas, 1998, 5, 2010-2021.	1.9	54
11	Four-dimensional GPS imaging of space weather storms. Space Weather, 2007, 5, n/a-n/a.	3.7	53
12	lonospheric data assimilation and forecasting during storms. Journal of Geophysical Research: Space Physics, 2016, 121, 764-778.	2.4	51
13	A three-dimensional time-dependent algorithm for ionospheric imaging using GPS. Annals of Geophysics, 2010, 46, .	1.0	51
14	Scintillationâ€producing Fresnelâ€scale irregularities associated with the regions of steepest TEC gradients adjacent to the equatorial ionization anomaly. Journal of Geophysical Research, 2010, 115, .	3.3	47
15	Interhemispheric comparison of GPS phase scintillation at high latitudes during the magnetic-cloud-induced geomagnetic storm of 5–7 April 2010. Annales Geophysicae, 2011, 29, 2287-2304.	1.6	45
16	Ionospheric scintillation over Antarctica during the storm of 5–6 April 2010. Journal of Geophysical Research, 2012, 117, .	3.3	45
17	GPS phase scintillation associated with optical auroral emissions: First statistical results from the geographic South Pole. Journal of Geophysical Research: Space Physics, 2013, 118, 2490-2502.	2.4	45
18	Development of Space Weather Reasonable Worst ase Scenarios for the UK National Risk Assessment. Space Weather, 2021, 19, e2020SW002593.	3.7	41

#	Article	IF	CITATIONS
19	Medical imaging and physiological modelling: linking physics and biology. BioMedical Engineering OnLine, 2009, 8, 1.	2.7	39
20	A comparison of reconstruction techniques used in ionospheric tomography. Radio Science, 1998, 33, 1767-1779.	1.6	38
21	GPS scintillation and TEC gradients at equatorial latitudes in April 2006. Advances in Space Research, 2011, 47, 1750-1757.	2.6	38
22	lonospheric delay corrections for single-frequency GPS receivers over Europe using tomographic mapping. GPS Solutions, 2009, 13, 141-151.	4.3	37
23	Annual Occurrence Rates of Ionospheric Polar Cap Patches Observed Using Swarm. Journal of Geophysical Research: Space Physics, 2018, 123, 2327-2335.	2.4	36
24	Determination of the vertical electron-density profile in ionospheric tomography: experimental results. Annales Geophysicae, 1997, 15, 747-752.	1.6	33
25	Wavelet analysis of GPS amplitude scintillation: A case study. Radio Science, 2007, 42, n/a-n/a.	1.6	33
26	Isolating the multipath component in GNSS signalâ€toâ€noise data and locating reflecting objects. Radio Science, 2011, 46, .	1.6	32
27	lonospheric effects of magnetopause reconnection observed using ionospheric tomography. Geophysical Research Letters, 1998, 25, 293-296.	4.0	30
28	The Use of GPS Measurements for Water Vapor Determination. Bulletin of the American Meteorological Society, 2003, 84, 1249-1258.	3.3	28
29	Identification of scintillation signatures on GPS signals originating from plasma structures detected with EISCAT incoherent scatter radar along the same line of sight. Journal of Geophysical Research: Space Physics, 2017, 122, 916-931.	2.4	28
30	GPS scintillation over the European Arctic during the November 2004 storms. GPS Solutions, 2008, 12, 281-287.	4.3	26
31	lonospheric storm time dynamics as seen by GPS tomography and in situ spacecraft observations. Journal of Geophysical Research, 2008, 113, .	3.3	25
32	A comparison of techniques for mapping total electron content over Europe using GPS signals. Radio Science, 2004, 39, n/a-n/a.	1.6	24
33	Probing the high latitude ionosphere from ground-based observations: The state of current knowledge and capabilities during IPY (2007–2009). Journal of Atmospheric and Solar-Terrestrial Physics, 2008, 70, 2293-2308.	1.6	23
34	Statistical analysis of travelling ionospheric disturbances using TEC observations from geostationary satellites. Journal of Atmospheric and Solar-Terrestrial Physics, 2012, 74, 64-80.	1.6	22
35	A comparison of the effects of initializing different thermosphereâ€ionosphere model fields on storm time plasma density forecasts. Journal of Geophysical Research: Space Physics, 2013, 118, 7329-7337.	2.4	22
36	A 12year comparison of MIDAS and IRI 2007 ionospheric Total Electron Content. Advances in Space Research, 2012, 49, 1348-1355.	2.6	20

#	Article	IF	CITATIONS
37	Observations of the F region height redistribution in the storm-time ionosphere over Europe and the USA using GPS imaging. Geophysical Research Letters, 2006, 33, n/a-n/a.	4.0	19
38	Imaging of 3â€Ð plasmaspheric electron density using GPS to LEO satellite differential phase observations. Radio Science, 2011, 46, .	1.6	19
39	A study of Lâ€band scintillations and total electron content at an equatorial station, Lagos, Nigeria. Radio Science, 2012, 47, .	1.6	19
40	Ionospheric corrections for GPS time transfer. Radio Science, 2014, 49, 196-206.	1.6	19
41	Imaging of fast moving electron-density structures in the polar cap. Annals of Geophysics, 2009, 50, .	1.0	19
42	Imaging the topside ionosphere and plasmasphere with ionospheric tomography using COSMIC GPS TEC. Journal of Geophysical Research: Space Physics, 2016, 121, 817-831.	2.4	18
43	EISCAT verification in the development of ionospheric tomography. Annales Geophysicae, 1996, 14, 1413-1421.	1.6	17
44	The use of ionosondes in GPS ionospheric tomography at low latitudes. Journal of Geophysical Research, 2012, 117, .	3.3	17
45	Correlation between scintillation indices and gradient drift wave amplitudes in the northern polar ionosphere. Journal of Geophysical Research, 2009, 114, .	3.3	16
46	Tomographic imaging of the equatorial and low-latitude ionosphere over central-eastern Brazil. Earth, Planets and Space, 2011, 63, 129-138.	2.5	16
47	GPS phase scintillation at high latitudes during geomagnetic storms of 7–17 March 2012 – Part 2: Interhemispheric comparison. Annales Geophysicae, 2015, 33, 657-670.	1.6	16
48	Application of radio tomographic imaging to HF oblique incidence ray tracing. Radio Science, 2001, 36, 1591-1598.	1.6	15
49	Electron density profiles determined from tomographic reconstruction of total electron content obtained from GPS dual frequency data: first results from the South African network of dual frequency GPS receiver stations. Advances in Space Research, 2004, 34, 2049-2055.	2.6	15
50	Use of radio-occultation data for ionospheric imaging during the April 2002 disturbances. GPS Solutions, 2005, 9, 156-163.	4.3	15
51	A multi-diagnostic approach to understanding high-latitude plasma transport during the Halloween 2003 storm. Annales Geophysicae, 2008, 26, 2739-2747.	1.6	15
52	lonospheric data assimilation applied to HF geolocation in the presence of traveling ionospheric disturbances. Radio Science, 2017, 52, 829-840.	1.6	15
53	GPS scintillations and total electron content climatology in the southern low, middle and high latitude regions. Annals of Geophysics, 2013, 56, .	1.0	15
54	A simulation study into constructing of the sample space for ionospheric imaging. Journal of Atmospheric and Solar-Terrestrial Physics, 2005, 67, 1085-1091.	1.6	14

#	Article	IF	CITATIONS
55	GPS interfrequency biases and total electron content errors in ionospheric imaging over Europe. Radio Science, 2006, 41, n/a-n/a.	1.6	14
56	Ionospheric imaging in Africa. Radio Science, 2014, 49, 19-27.	1.6	14
57	Polar cap plasma patch primary linear instability growth rates compared. Journal of Geophysical Research: Space Physics, 2016, 121, 3439-3451.	2.4	14
58	Measurement of Ionospheric Total Electron Content Using Singleâ€Frequency Geostationary Satellite Observations. Radio Science, 2019, 54, 10-19.	1.6	14
59	Detrend effect on the scalograms of GPS power scintillation. Advances in Space Research, 2009, 43, 1740-1748.	2.6	13
60	lonospheric response to the corotating interaction region–driven geomagnetic storm of October 2002. Journal of Geophysical Research, 2009, 114, .	3.3	13
61	Turbulent times in the northern polar ionosphere?. Journal of Geophysical Research, 2010, 115, .	3.3	13
62	The use of ionospheric tomography and elevation masks to reduce the overall error in single-frequency GPS timing applications. Advances in Space Research, 2011, 47, 276-288.	2.6	13
63	Imaging space weather over Europe. Space Weather, 2013, 11, 69-78.	3.7	13
64	A study into the errors in vertical total electron content mapping using GPS data. Radio Science, 2006, 41, n/a-n/a.	1.6	12
65	Imaging of the Antarctic ionosphere: Experimental results. Journal of Atmospheric and Solar-Terrestrial Physics, 2009, 71, 1757-1765.	1.6	12
66	The effects of receiver location in two-station experimental ionospheric tomography. Journal of Atmospheric and Solar-Terrestrial Physics, 1997, 59, 1411-1415.	1.6	11
67	Simultaneous observations of the main trough using GPS imaging and the EISCAT radar. Annales Geophysicae, 2005, 23, 753-757.	1.6	11
68	High-latitude ionospheric response to co-rotating interaction region- and coronal mass ejection-driven geomagnetic storms revealed by GPS tomography and ionosondes. Proceedings of the Royal Society A: Mathematical, Physical and Engineering Sciences, 2010, 466, 3391-3408.	2.1	11
69	Further observations of GPS satellite oscillator anomalies mimicking ionospheric phase scintillation. GPS Solutions, 2014, 18, 387-391.	4.3	11
70	Threeâ€dimensional modeling of highâ€latitude scintillation observations. Radio Science, 2016, 51, 1022-1029.	1.6	11
71	A multiresolution inversion for imaging the ionosphere. Journal of Geophysical Research: Space Physics, 2017, 122, 6799-6811.	2.4	11
72	Multi-instrument probing of the polar ionosphere under steady northward IMF. Annales Geophysicae, 2000, 18, 90-98.	1.6	10

#	Article	IF	CITATIONS
73	Validation of electron density profiles derived from oblique ionograms over the United Kingdom. Radio Science, 2001, 36, 1149-1156.	1.6	10
74	New iterative cone beam CT reconstruction software: Parameter optimisation and convergence study. Computer Methods and Programs in Biomedicine, 2010, 100, 166-174.	4.7	10
75	A motion-compensated cone-beam CT using electrical impedance tomography imaging. Physiological Measurement, 2011, 32, 19-34.	2.1	10
76	Using sparse regularization for multi-resolution tomography of the ionosphere. Nonlinear Processes in Geophysics, 2015, 22, 613-624.	1.3	10
77	A realistic simulation framework to evaluate ionospheric tomography. Advances in Space Research, 2020, 65, 891-901.	2.6	10
78	GPS loss of lock statistics over Brazil during the 24th solar cycle. Advances in Space Research, 2020, 66, 219-225.	2.6	10
79	An interhemispheric comparison of GPS phase scintillation with auroral emission observed at the South Pole and from the DMSP satellite. Annals of Geophysics, 2013, 56, .	1.0	10
80	GPS satellite oscillator faults mimicking ionospheric phase scintillation. GPS Solutions, 2012, 16, 477-482.	4.3	9
81	Passive, continuous monitoring of carbon dioxide geostorage using muon tomography. Philosophical Transactions Series A, Mathematical, Physical, and Engineering Sciences, 2019, 377, 20180059.	3.4	9
82	The correction for the satellite-receiver longitude difference in ionospheric tomography. Journal of Atmospheric and Solar-Terrestrial Physics, 1997, 59, 2077-2087.	1.6	8
83	Comparison of 4D tomographic mapping versus thin-shell approximation for ionospheric delay corrections for single-frequency GPS receivers over North America. GPS Solutions, 2010, 14, 279-291.	4.3	8
84	GPS tomography in the polar cap: comparison with ionosondes and in situ spacecraft data. GPS Solutions, 2011, 15, 79-87.	4.3	8
85	Horseshoes in the Highâ€Latitude Ionosphere. Journal of Geophysical Research: Space Physics, 2018, 123, 5831-5849.	2.4	7
86	Tomographic Imaging of Traveling Ionospheric Disturbances Using GNSS and Geostationary Satellite Observations. Journal of Geophysical Research: Space Physics, 2020, 125, e2019JA027551.	2.4	7
87	EISCAT verification in the development of ionospheric tomography. Annales Geophysicae, 1996, 14, 1413.	1.6	7
88	Imaging of near-Earth space plasma. Philosophical Transactions Series A, Mathematical, Physical, and Engineering Sciences, 2002, 360, 2805-2818.	3.4	6
89	Improving the vertical electron density profile in ionospheric imaging at storm time: A case study on 25–27 September 2011. Journal of Geophysical Research: Space Physics, 2014, 119, 7963-7971.	2.4	6
90	On the Annual Asymmetry of High‣atitude Sporadic F. Space Weather, 2019, 17, 1618-1626.	3.7	6

#	Article	IF	CITATIONS
91	Rapid and Accurate Measurement of Polarization and Fading of Weak VHF Signals Obliquely Reflected From Sporadic-E Layers. IEEE Transactions on Antennas and Propagation, 2021, 69, 4033-4048.	5.1	6
92	Coordinated Ionospheric Reconstruction CubeSat Experiment (CIRCE) mission overview. , 2019, , .		6
93	Demonstration of the use of the Doppler Orbitography and Radio positioning Integrated by Satellite (DORIS) measurements to validate GPS ionospheric imaging. Advances in Space Research, 2011, 48, 500-506.	2.6	5
94	Comparison of temporal fluctuations in the total electron content estimates from EISCAT and GPS along the same line of sight. Annales Geophysicae, 2013, 31, 745-753.	1.6	5
95	Towards adapting a normal patient database for SPECT brain perfusion imaging. Inverse Problems, 2012, 28, 065001.	2.0	4
96	Analysis of the Regional lonosphere at Low Latitudes in Support of the Biomass ESA Mission. IEEE Transactions on Geoscience and Remote Sensing, 2018, 56, 6412-6424.	6.3	4
97	Verification of CHAMP Radio-Occultation Observations in the Ionosphere Using MIDAS. , 2003, , 545-550.		4
98	Consolidated Amateur Radio Signal Reports as Indicators of Intense Sporadic E Layers. Atmosphere, 2022, 13, 906.	2.3	4
99	lonospheric imaging at mid-latitudes using both GPS and ionosondes. Journal of Atmospheric and Solar-Terrestrial Physics, 2007, 69, 817-825.	1.6	3
100	Analysis of diurnal double maxima observed above Italy during 1975–1991. Journal of Atmospheric and Solar-Terrestrial Physics, 2012, 89, 67-75.	1.6	3
101	Quality analysis of dual-frequency smartphone-based ionospheric TEC measurements: what can be achieved?. Annals of Geophysics, 2020, 63, .	1.0	3
102	<i>Letter to the Editor:</i> First complementary observations by ionospheric tomography, the EISCAT Svalbard radar and the CUTLASS HF radar. Annales Geophysicae, 1998, 16, 1519-1522.	1.6	2
103	New method for tracking the movement of ionospheric plasma. Journal of Geophysical Research, 2012, 117, .	3.3	2
104	Robust ionospheric tomography using sparse regularization. , 2014, , .		2
105	Measuring GNSS ionospheric total electron content at Concordia, and application to L-band radiometers. Annals of Geophysics, 2013, 56, .	1.0	2
106	Ionization dynamics during storms of the recent Solar Maximum. Geophysical Monograph Series, 2008, , 83-90.	0.1	1
107	Image-model coupling: a simple information theoretic perspective for image sequences. Nonlinear Processes in Geophysics, 2009, 16, 197-210.	1.3	1
108	A dual modality of cone beam CT and electrical impedance tomography for lung imaging. Journal of Physics: Conference Series, 2010, 224, 012026.	0.4	1

#	Article	IF	CITATIONS
109	Image-model coupling: application to an ionospheric storm. Nonlinear Processes in Geophysics, 2010, 17, 361-369.	1.3	1
110	ANIMo $\hat{a} \in$ " A New Ionospheric Model. Ionospheric Modeling for Ionospheric Imaging and Forecasting Purposes. , 0, , .		1
111	Method to measure the Stokes parameters of GPS signals. Radio Science, 2014, 49, 7-18.	1.6	1
112	A comparison of the relative effect of the Earth's quasiâ€DC and AC electric field on gradient drift waves in largeâ€scale plasma structures in the polar regions. Journal of Geophysical Research: Space Physics, 2016, 121, 9012-9019.	2.4	1
113	GPS phase scintillation and auroral electrojet currents during geomagnetic storms of March 17, 2013 and 2015. , 2017, , .		1
114	The use of GLONASS data in ionospheric imaging over the Antarctic. , 2011, , .		0
115	Multiresolution Tomography of Ionospheric Electron Density. , 2014, , .		0
116	Implementation of a new ionospheric model (ANIMo) into a three-dimensional variational analysis (3D-Var) for imaging and forecasting purposes. , 2014, , .		0
117	Space-Plasma Imaging — Past, Present and Future. Series on Iraq War and Its Consequences, 2007, , 93-108.	0.1	0